Journal of Ceramic Processing Research. Vol. 25, No. 4, pp. 475~482 (2024)
(Received 25 May 2024, Received in revised form 5 July 2024, Accepted 16 July 2024)
https://doi.org/10.36410/jcpr.2024.25.4.475

J O U R N A L O F
Ceramic Processing Research

Controlling luminescent characteristics of ZASN glass-ceramics through tailored crystallization mechanism and processing

Jihyeon Yun and Seunggu Kang*
Department of Advanced Material Engineering, Kyonggi University, Suwon, Kyonggi-do 16227, Korea

The ZnO-Al_2O_3-SiO_2-Na_2O (ZASN) system glass was fabricated and heat-treated to produce glass-ceramics specimens containing willemite (Zn_2SiO_4). The obtained glass revealed the presence of minor phase-separated droplets, each tens of nanometers in size, serving as nuclei for crystal growth and enabling a direct one-step heat treatment process without the need for a separate nucleation step. The activation energy (E) for crystallization was calculated from DTA data using the Kissinger equation. The resulting Avrami constant (n) was found to be 1.49 when substituted E into the Augis-Bennett equation, indicating surface nucleation, which suggests that controlling the size and distribution of droplets could enhance the properties of glass-ceramics through induced internal crystallization. Photoluminescence (PL) properties revealed broad emission peaks attributed to Zn^{2+} ions with d10 electronic configuration. CIE color coordinate of glass-ceramics treated within 10 minutes shifted towards darker blue hues with time; exceeding 1 hour shifted towards cyan. The controllability of crystallization mechanism and heat treatment process in ZASN glass, along with fine adjustability of luminescent properties, suggests potential for applications in cyan-green luminescent materials.

Keywords: ZASN system, Glass-ceramics, Willemite, Crystallization mechanism, Photoluminescence.

Introduction

Glass is an amorphous solid with a glass transition temperature (T_g), at which the supercooled liquid state transitions into a solid state. Within glass, atoms or molecules exist in a disordered state. However, through appropriate heat treatment processes, crystals with specific properties can be precipitated within the glass, enhancing its characteristics. This process of inducing the precipitation of specific crystalline phases within amorphous glass to improve its properties results in what is known as glass-ceramics.

Glass-ceramics retain the excellent workability and productivity of glass while also possessing the superior physical, mechanical, and chemical properties of crystalline solids. One of the key advantages of glass-ceramics is the ability to freely control the type, fraction, shape, and size of precipitated crystalline phases by adjusting the composition and processing parameters. Due to these advantages, glass-ceramics can effectively meet the diverse demands of modern society, and research on glass-ceramics continues to be actively pursued [1-8].

Glass containing ZnO is known to have superior mechanical properties and a lower softening point compared to typical glass [9-12]. Additionally, ZnO-containing glass exhibits high transparency across the ultraviolet to infrared spectrum, low refractive index, and high thermal stability. It can also display unique optical properties when doped with various ions, making it suitable for a wide range of applications [9,13-15]. Among these, the willemite (Zn_2SiO_4) crystalline phase, obtained from ZnO-SiO_2 system glass, has three polymorphs: α-willemite, known for its green luminescence, β-willemite, known for its yellow luminescence, and γ-willemite, known for its red luminescence [16-23].

Elements with a d10 electronic configuration, such as Zn^{2+}, are known to form a broad emission band in the cyan spectrum depending on the composition of the host glass [18]. Moreover, doping willemite with rare earth or transition metals results in luminescence across a broad range of visible and near-infrared wavelengths. This doping enhances luminescence efficiency, chromaticity, and provides high chemical and thermal stability, making willemite a practical phosphor used in various industrial applications [16, 17, 24-30]. Therefore, using willemite-based glass-ceramics as hosts for various luminescent materials can be applied in laser crystals, phase transition luminescent materials, displays, and lighting devices [24, 31-37]. Additionally, willemite-based glass-ceramics are important crystalline glazes utilized in the modern ceramics industry [38, 39].

Due to the continuous commercial demand for luminescent materials, extensive research has been conducted on excellent luminophores hosted by willemite glass-ceramics. However, most studies have focused on

*Corresponding author:
Tel : +82-31-249-9767
Fax: +82-31-249-9774
E-mail: sgkang@kyonggi.ac.kr

cases where rare earth or transition metals are doped, while research on pure willemite glass-ceramics has been relatively limited.

Therefore, in this study, in order to investigate pure willemite glass-ceramics, we designed a ZnO-Al_2O_3-SiO_2-Na_2O (ZASN) system glass without the addition of rare earth or transition metals. By utilizing phase separation in glass samples, we were able to produce glass-ceramics through a one-step heat treatment method without going through the nucleation stage. We then observed the generated crystalline phase, crystallization behavior, and microstructural changes according to the heat treatment time variable. Additionally, we analyzed the photoluminescence (PL) characteristics of the glass-ceramics to identify the emission wavelength range and studied the color characteristics of luminescence through CIE coordinate analysis.

Experimentals

Glass Preparation

In this study, ZnO (99.99%, Kojundo chemicals, Ltd., Japan), Al_2O_3 (99.99%, Kojundo chemicals, Ltd., Japan), SiO_2 (99.99%, Kojundo chemicals, Ltd., Japan) and Na_2CO_3 (99.99%, Kojundo chemicals, Ltd., Japan) were used as raw materials for glass production. The glass composition employed in this study was $38.95ZnO$-$7.6Al_2O_3$-$48.45SiO_2$-$5Na_2O$ (mol%), and the oxide materials were mixed according to this composition ratio and dry ball-milled for 12 h at 120 rpm with zirconia balls. The mixed powder, after completion of mixing and grinding via ball-milling, was placed into an alumina crucible and melted at 1450°C for 2 h using an electric furnace. The molten glass was poured into preheated graphite molds at 400°C under atmospheric conditions for quenching and subsequently annealed for 1 h to minimize internal stress within the glass, preventing breakage. The glass was then naturally cooled to room temperature to obtain the parent glass. Glass-ceramics were prepared by heating the obtained parent glass at a rate of 10°C/min to 792°C using an electric furnace, holding at this temperature for various heat treatment times (1 min, 5 min, 10 min, 30 min, 1 h, 2 h, and 4 h), and then naturally cooled.

Analysis

The manufactured glass was crushed and particles below 45 μm were selected for thermal characterization using a differential thermal analyzer (DTA, STA449 F3, NETZSCH, Germany) with a heating rate of 10°C/min. In particular, DTA analysis was performed on the glass at various heating rates (5, 10, 15, 20°C/min) to calculate the Avrami constant, which provides insight into the crystallization mechanism. Analysis of the crystalline phases in the glass-ceramics was conducted using X-ray diffraction (XRD, MiniFlex II, Rigaku Co., Japan) in the range of 5° to 90° using Cu-Kα (1.5406 Å) radiation. The microstructure of the glass was examined through scanning electron microscope (SEM, Nova NanoSEM 200, FEI, USA) analysis. Specimens for SEM observation were polished to a mirror-like flatness level using SiC paper and diamond suspension. Subsequently, etching was performed for 3 seconds in a 3% HF solution to facilitate clear observation of the crystalline phases.

The luminescent properties of the manufactured glass were analyzed using a photoluminescence measurement instrument (PL, PSI, Darsa-5000). In this process, a 500 W Xenon lamp was used as the excitation source, and the emission wavelength was measured in the range of 380-780 nm. The emitted light analyzed through PL was further examined for color characteristics using CIE (Commission Internationale de l'Eclairage) color coordinates.

Results and Discussions

Figure 1 shows the results of the DTA analysis of the ZASN system parent glass. The glass transition temperature (T_g) was observed at 653°C, with two prominent exothermic peaks. The exothermic peaks during glass heating indicate crystallization initiation. The onset temperature (T_{c1}) for crystallization initiation at the first exothermic peak was 771°C, and the peak temperature (T_{p1}) for maximum crystallization growth was 792°C. At the second exothermic peak, the onset temperature (T_{c2}) for crystallization initiation was 981°C, and the peak temperature (T_{p2}) for maximum crystallization growth was 999°C. Typically, willemite crystalline phase is known to manifest α-willemite at temperatures around 800°C [20,24]. Hence, in this study, glass-ceramics were produced by performing heat treatment at a temperature similar to the crystallization temperature of α-willemite,

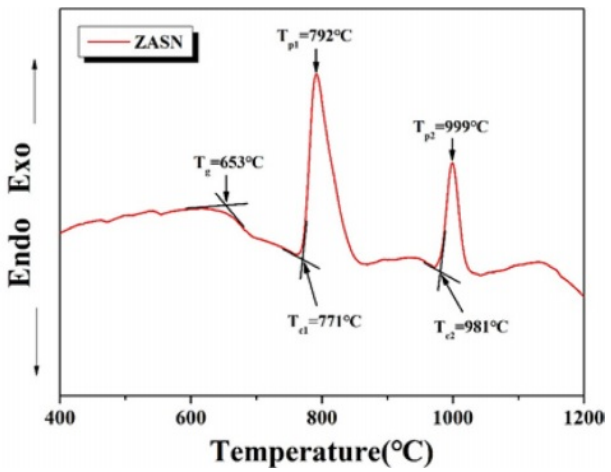

Fig. 1. DTA graph of ZASN system parent glass with heating rate of 10 min/°C. T_g represents the glass transition temperature, while T_{c1} and T_{p1} denote the onset and peak temperatures of the first crystallization peak, and T_{c2} and T_{p2} represent the onset and peak temperatures of the second crystallization peak.

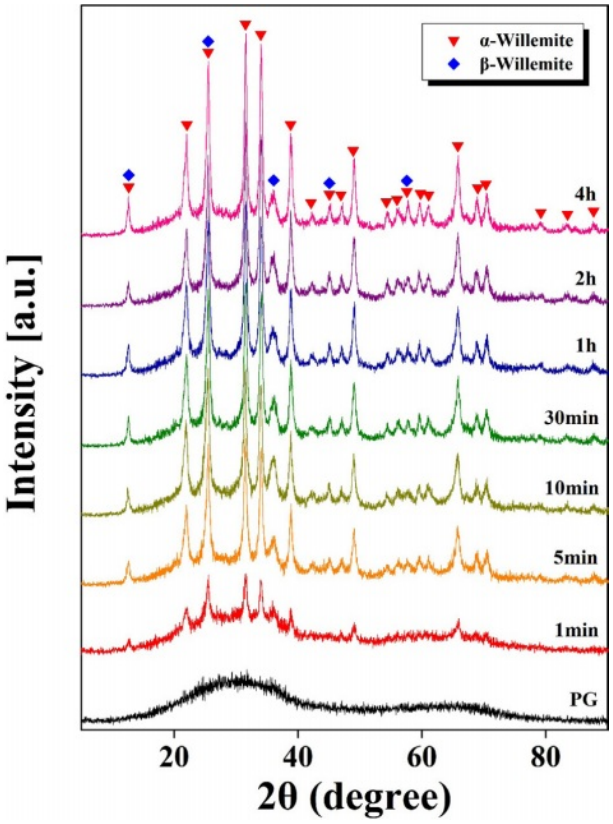

Fig. 2. XRD graph of ZASN parent glass and glass-ceramics heat-treated at 792°C as a function of time.

namely T_{p1} at 792°C.

In Fig. 2, the XRD analysis results of the glass-ceramics samples treated at 792°C for various durations are presented. The parent glass exhibited a completely amorphous state, showing only a gentle hill-shaped spectrum without any crystalline peaks. In contrast, both α-willemite and β-willemite peaks were observed in all samples subjected to heat treatment. Until a heat treatment duration of 10 minutes, the intensity of each crystal increased distinctly with time. However, beyond 10 minutes of heat treatment, no further increase in peak intensity was observed.

Figure 3 shows the SEM observations of the ZASN parent glass and glass-ceramics. In the 3,000x magnification image of the parent glass, no fine structures were observed, whereas in the image magnified to 50,000x (image within the square box in (a)), spherical particles ranging from 20 to 40 nm in size were evenly distributed within the matrix. These nanoscale particles could either be fine crystals [18] or minor phases resulting from phase separation.

Since the glass was melted at a high temperature of 1450°C and quenched, it is considered unlikely to contain fine crystals. Therefore, the observed spherical particles at the nanometer scale are presumed to be minor phases resulting from phase separation. We conducted an EDS analysis to determine the composition of the nanoparticles. However, we did not observe clear compositional differences between the spherical particles and the surrounding phases within 1 atomic %. Therefore, future analyses will require more precise EDS instrumentation to accurately determine nanoparticle composition.

Typically, the boundaries between two phases are unstable and possess high energy [40]. The boundary between the spherical phase and the matrix in this glass is also expected to have high energy, providing sites where surrounding atoms can easily move and bond, thus serving as nuclei for crystal growth. Unlike other glasses that generally require the introduction of oxides or metal colloids or the use of F^- ions for nucleation, ZASN glass system induce phase separation in the composition itself without the need for additional nucleation agents, making them advantageous in that a one-step heat treatment process can be applied [41, 42].

The crystals formed in the glass-ceramics are all spherical, and based on the XRD results as shown in Fig. 2, these crystalline phases can be identified as willemite. This spherical willemite formation is consistent with observations made by other researchers [25, 31]. Fig. 4 illustrates the change in crystal size according to the heat treatment time. In the initial stage, within 15 min of heat treatment, the relationship is linear, but after 30 min, the crystal size converges to approximately 25 μm, indicating that crystal growth halts. From the slope of the linear portion during the initial heat treatment, the crystal growth rate was calculated to be 3.20 μm/min.

Growth of the crystals occurred with increasing heat treatment time in the range of 1 min to 30 min. However, when the heat treatment time exceeded 1 hour, the crystal size no longer increased. This cessation in growth is attributed to the crystals growing from the glass matrix coming into contact with each other, thereby no longer providing additional space for growth and the parent glass is depleted. This can be explained by the following mechanism.

Typically, when glass is heat-treated, crystalline phases are commonly formed through two mechanisms: one is surface crystallization, where crystals predominantly grow on the surface of the glass specimen, and the other is bulk crystallization, where crystals predominantly grow within the specimen. When glass is heated at a constant temperature for time t, crystals begin to form and grow, gradually reducing the remaining amount of parent glass. Assuming that nucleation and crystal growth occur at a constant rate, the volume fraction x of the crystalline phase over time is given by the Johnson-Mehl-Avrami (JMA) equation as shown in Eq. (1) [43, 44].

$$x = 1 - \exp(-kt^n) \tag{1}$$

Here, n is a constant determined by the crystallization mechanism, known as the Avrami constant, and k is a constant depending on the nucleation and crystal growth

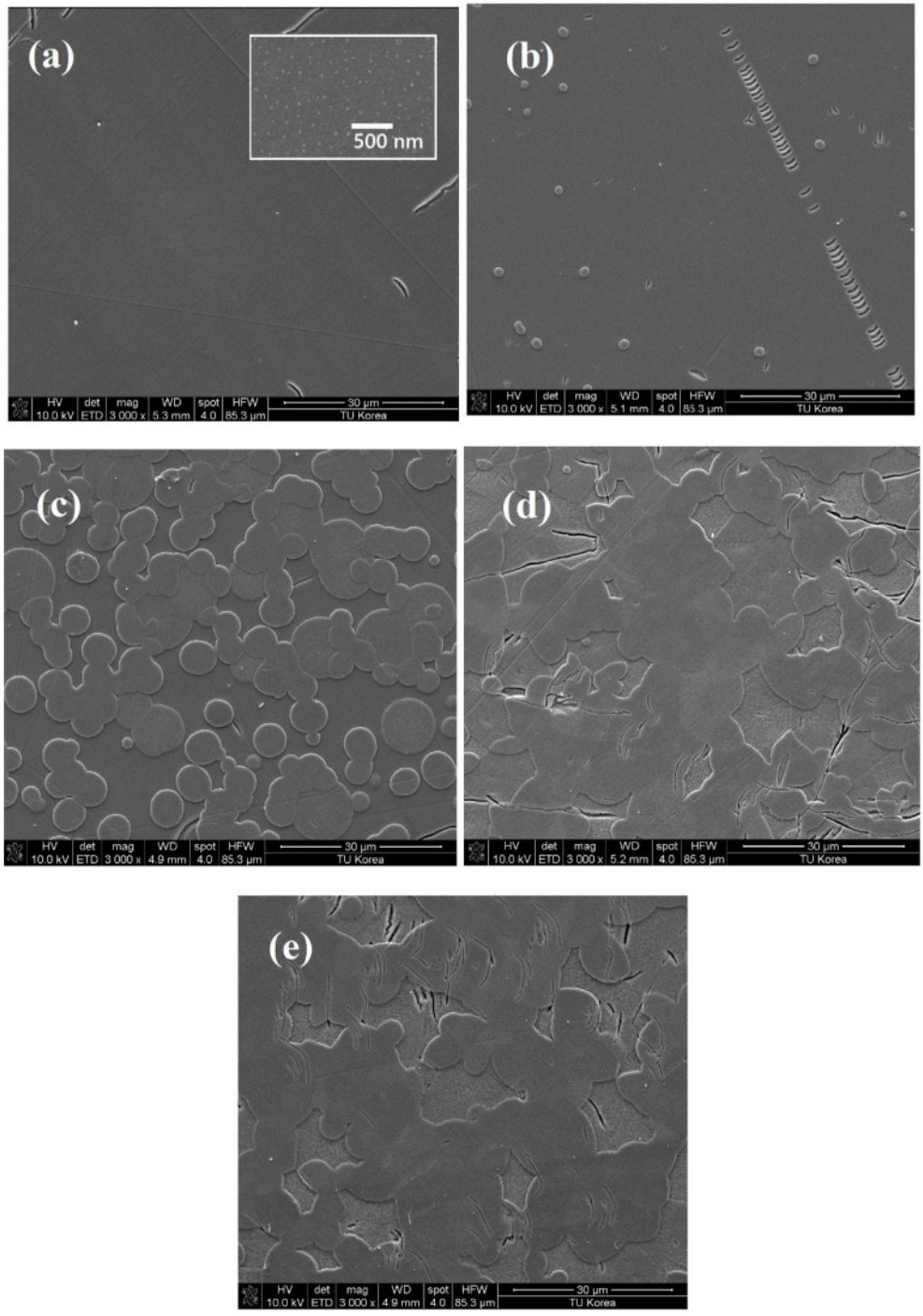

Fig. 3. SEM images of (a) parent glass and glass-ceramic heat-treated for (b) 1 minute, (c) 5 minutes, (d) 30 minutes, and (e) 1 hour. The scale for all images is 3,000x. However, the scale for the inset image within figure (a) is 50,000x.

rates.

Usually, the value of n falls between 1 and 5, where a value close to 1 indicates predominance of surface crystallization, while values above 4 suggest dominance of bulk crystallization.

The value of n can be easily determined using the equation proposed by Augis-Bennett (Eq. 2) [45, 46].

$$n = \frac{2.5}{\Delta T_{FWHM}} \times \frac{RT_P^2}{E} \tag{2}$$

Here, ΔT_{FWHM} is the full width at half maximum of the exothermic peak in the DTA graph of the parent glass, T_p is the temperature of this exothermic peak (maximum crystallization temperature), R is the gas constant, and E is the activation energy required for crystallization.

To determine the activation energy E, the equation proposed by Kissinger (Eq. 3) must be used [47].

$$\ln\left(\frac{\alpha}{T_P^2}\right) = \left(\frac{-E}{RT_P}\right) + const. \tag{3}$$

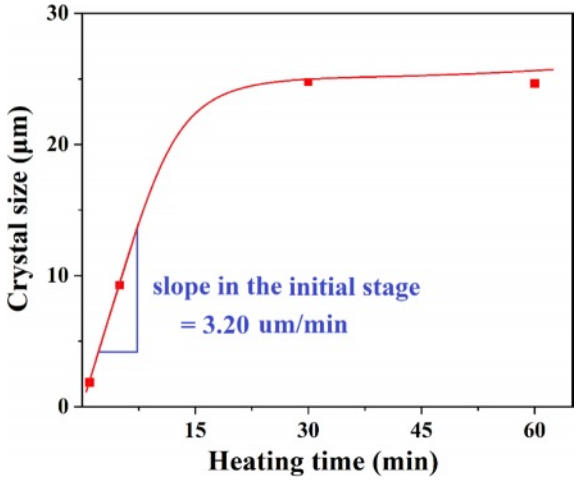

Fig. 4. Crystal size plotted against heat treatment time. Initially, a linear relationship is observed, but after 30 minutes, the crystal size stabilizes at around 25 μm, indicating cessation of crystal growth. The calculated crystal growth rate during the initial stage of heat treatment was 3.20 μm/min.

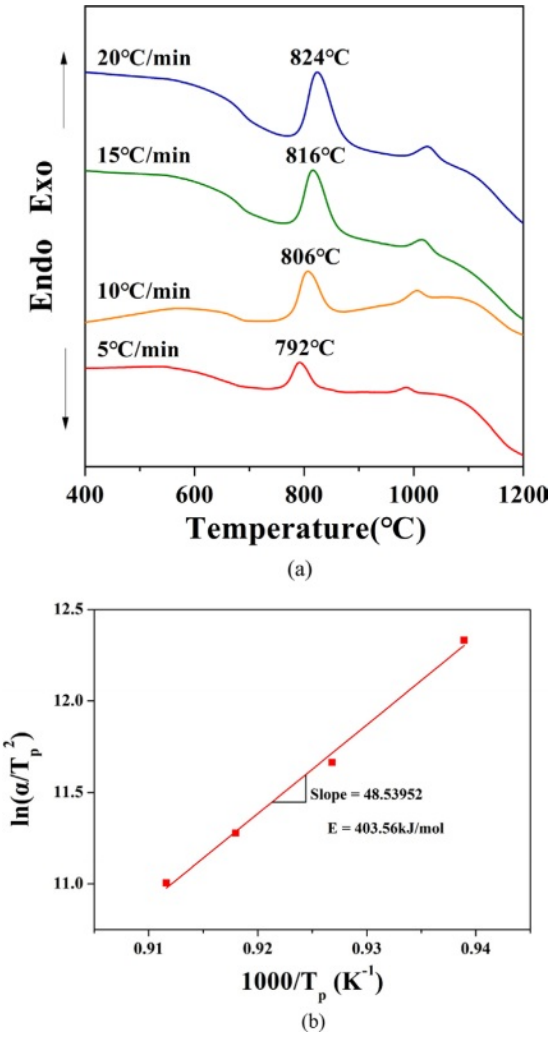

Fig. 5. (a) DTA graph of parent glass with varying heating rates, (b) linear correlation between $1{,}000/T_p$ and $\ln(\alpha/T_p^2)$, indicating the activation energy for crystal growth as 403.56 kJ/mol.

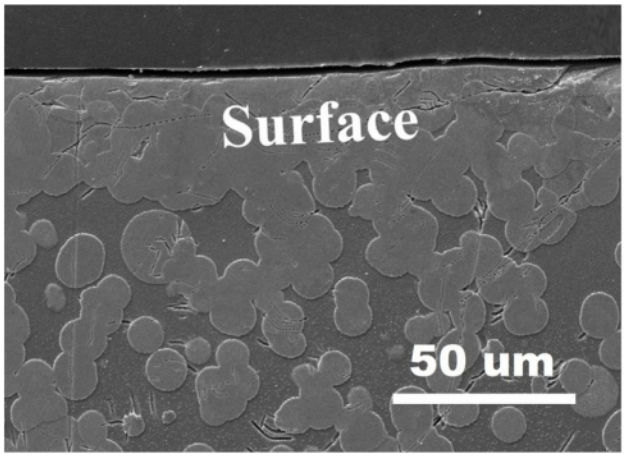

Fig. 6. SEM cross-section of glass-ceramic heat-treated for 10 minutes, showing dense surface crystallization, with predominant surface over bulk crystallization.

Here, α is the heating rate during DTA analysis, and R is the gas constant.

By performing DTA analysis on four parent glass samples at different heating rates of 5, 10, 15, and 20°C/min (Fig. 5(a)), and substituting the results into Eq. (3), a $1000/T_p$ vs. $\ln(\alpha/T_p^2)$ graph was plotted, as shown in Fig. 5(b). From the slope of this graph, the activation energy required for crystallization, 403.56 kJ/mol, was determined. Using the obtained E value in Eq. (2), the Avrami constant n was calculated to be 1.49. This value corresponds to surface crystallization, indicating that the ZASN glass composition prepared in this study exhibits surface crystallization behavior. Fig. 6 shows the SEM image of the cross-section of the glass-ceramics heat-treated for 10 minutes. Crystallization occurred very densely on the surface. Although crystallization also occurred in bulk, surface crystallization was more predominant than bulk crystallization in the specimen heat-treated for 10 minutes.

Figure 7(a) shows the photoluminescence (PL) spectra of both the parent glass and the glass-ceramics. When excited at a wavelength of 362 nm, broad band-shaped luminescent peaks were observed in the violet and cyan regions in all specimens. These luminescent peaks appeared at 412, 451, 469, 484, 546, 577, and 731 nm. The emergence of these luminescent peaks is attributed to the characteristic of the Zn^{2+} element with a d10 electron configuration, along with the luminescent effect of willemite crystalline phase occurring in combination [18]. However, the appearance of the peak at 731 nm is considered to be due to the excitation at a wavelength of 362 nm [48].

Figure 7(b) illustrates the changes in the intensity of the main luminescent peak at 412 nm in the PL spectra of the glass-ceramics as a function of heat treatment time. Initially, the peak intensity of the glass-ceramics heat-treated for 1 minute was approximately 6% higher than that of the parent glass. However, in

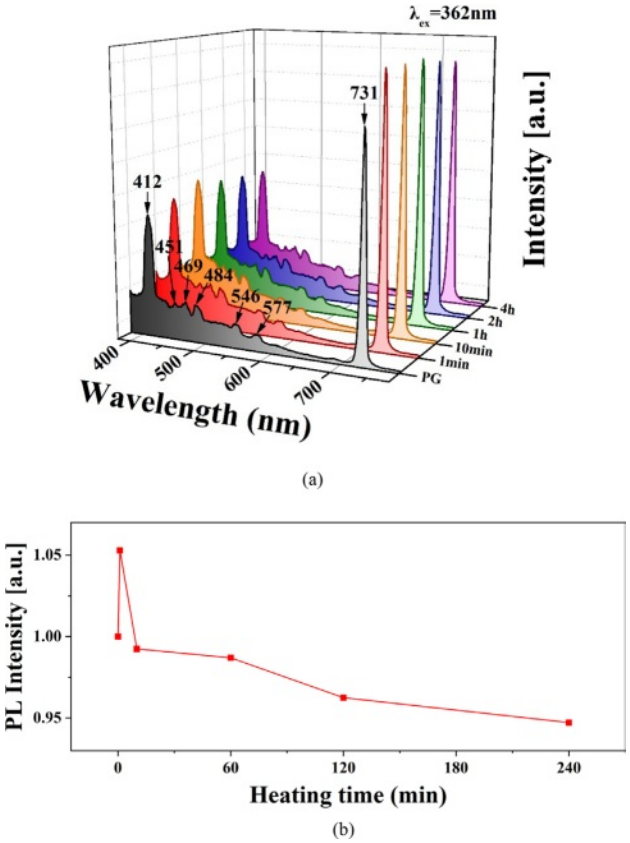

Fig. 7. (a) PL spectra of parent glass and glass-ceramics versus heating time. (b) Intensity change of the 412 nm luminescence peak during crystalline growth heat treatment.

specimens heat-treated for 10 minutes or more, the peak intensity decreased with increasing heat treatment time. For instance, the specimen heat-treated for 4 hours exhibited a peak intensity more than 5% lower than that of the parent glass. The luminescence intensity of the ZASN glass-ceramics treated for more than 10 minutes decreased compared to that of the parent glass. This decline in PL intensity is likely due to excessive crystal formation making the specimens opaque, which prevented the emitted light from escaping the specimens.

In Fig. 8, the information obtained from the PL spectra of ZASN parent glass and glass-ceramics is represented in the CIE color coordinates. Initially, the parent glass exhibited luminescence characteristics in the light blue region. Comparing with the parent glass, glass-ceramics treated for less than 10 minutes showed a shift in the luminescence coordinates towards the deeper blue side as the heat treatment time increased. However, when the heat treatment time exceeded 1 hour, the luminescence coordinates observed a shift back towards the light cyan side. Thus, it can be inferred that the ZASN-based glass-ceramics fabricated in this study allows for fine control of blue luminescence characteristics from light to dark depending on the heat treatment conditions.

Figure 9 displays photographs taken with an optical camera of ZASN parent glass and glass-ceramics heat-

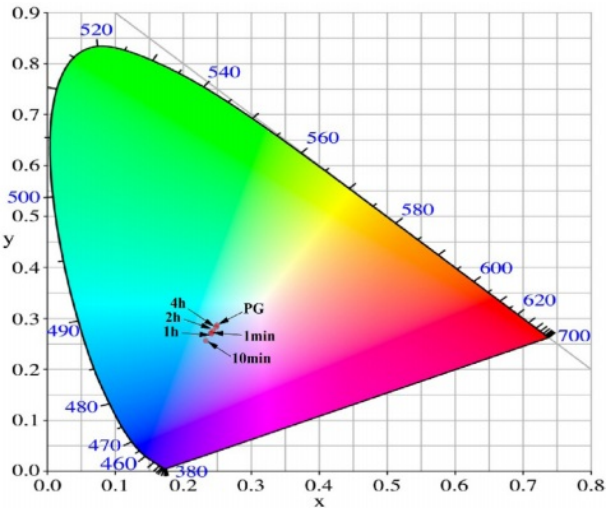

Fig. 8. Indication of CIE color coordinates for the emitted light from ZnO-Al_2O_3-SiO_2-Na_2O-based glass-ceramics as a function of heating time.

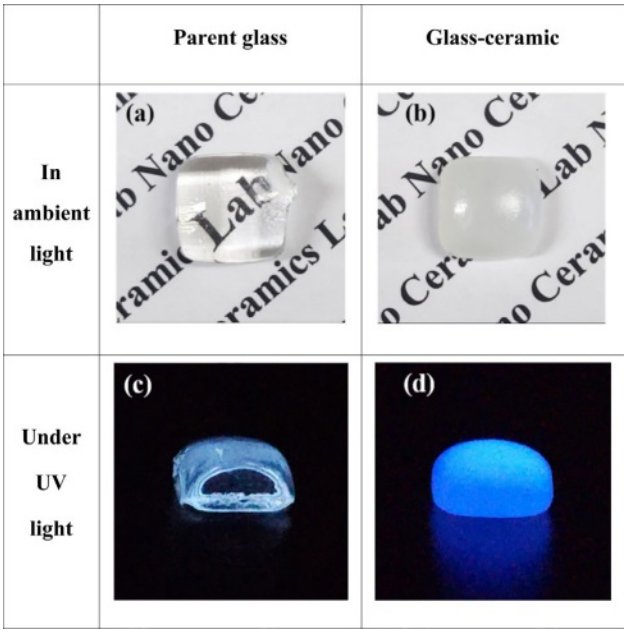

Fig. 9. (a) and (b) show the appearance of parent glass and glass-ceramic after 4 hours of heat treatment under ambient light; (c) and (d) depict the same specimens under 254 nm UV light in a dark room.

treated at 792°C for 4 hours. In ambient light, the parent glass appeared transparent, while the glass-ceramics exhibited an opaque opal-like appearance as shown in (a) and (b). Under 254 nm UV light in a dark room, both specimens emitted blue light as shown in (c) and (d).

Conclusion

In this study, we manufactured ZnO-Al_2O_3-SiO_2-Na_2O (ZASN) glass-ceramics with willemite crystalline phase and analyzed their crystallization mechanism and optical

properties. The glass transition temperature (T_g) of ZASN parent glass was 653°C, and the temperature for α-willemite manifestation was 792°C. Within the parent glass, phase separation occurred in the form of droplets with sizes in the tens of nanometers, acting as nuclei for crystal growth. The activation energy (E) required for crystallization of the parent glass was 403.56 kJ/mol, and the Avrami constant (n) was 1.49, indicating predominance of surface crystallization. Furthermore, in the ZASN glass-ceramic samples, broad-band luminescent peaks were observed in the violet and cyan regions during photoluminescence (PL) measurements, attributed to the characteristic of Zn^{2+} ions with a d10 electron configuration forming broad emission bands in the cyan spectral region. Glass-ceramics specimens heat-treated for less than 10 minutes exhibited a deep blue luminescent characteristic with increasing time, while those treated for over 1 hour showed a shift towards light cyan with increasing processing time, as revealed by CIE color coordinate analysis.

This study demonstrates the potential to enhance glass-ceramics properties by controlling droplet size and distribution during phase separation in ZASN parent glass, thus inducing bulk crystallization. Additionally, by controlling the crystallization mechanism and heat treatment process of glass-ceramics in the ZASN system, the ability to finely adjust luminescent properties within the blue to cyan range has been proven. Therefore, the samples obtained in this study show broad potential for future applications in blue-green luminescent materials.

Acknowledgement

This work was supported by Kyonggi University Research Grant 2021.

References

1. G.-H. Chen and X.-Y. Liu, J. Alloys Compd. 431[1-2] (2007) 282-286.
2. K.A. Almasri, H.A.A. Sidek, K.A. Matori, and M.H.M. Zaid, Results Phys. 7 (2017) 2242-2247.
3. H. Lin, T. Hu, Y. Cheng, M. Chen, and Y. Wang, Laser Photonics Rev. 12 (2018) 1700344.
4. A.S. Rao, J. Ashok, B. Suresh, G.N. Raju, N. Venkatramaiah, V.R. Kumar, I.V. Kityk, and N. Veeraiah, J. Alloys Compd. 712 (2017) 672-686.
5. F. Pei, G. Zhu, P. Li, H. Guo, and P. Yang, Ceram. Int. 46[11] (2020) 17825-17835.
6. Z. Tong, C. Xu, J. Wang, and Z. Jia, J. Ceram. Process. Res. 24[1] (2023) 17-28.
7. N. Kawaguchi and T. Yanagida, J. Ceram. Process. Res. 20[5] (2019) 455-459.
8. D. Shiratori, Y. Isokawa, H. Samizo, M. Koshimizu, N. Kawaguchi, and T. Yanagida, J. Ceram. Process. Res. 20[4] (2019) 301-306.
9. M.H.M. Zaid, K.A. Matori, S.H.A. Aziz, H.M. Kamari, Z.A. Wahab, Y.W. Fen, and I.M. Alibe, J. Mater. Sci. Mater. Electron. 27 (2016) 11158-11167.
10. A.M. Hu, M. Li, D.L.M. Dali, and K.M. Liang, Thermochim Acta 437[1-2] (2005) 110-113.
11. H. Gui, C. Li, C. Lin, Q. Zhang, Z. Luo, L. Han, J. Liu, T. Liu, and A. Lu, J. Eur. Ceram. Soc. 39[4] (2019) 1397-1410
12. S.A.A. Wahab, K.A. Matori, S.H.A. Aziz, M.H.M. Zaid, M.M.A. Kechik, A.Z.K. Azman, R.E.M. Khaidir, M.Z.A. Khiri, and N. Effendy, J. Mater. Res. Technol. 9[5] (2020) 11013-11021.
13. J. Hrabovsky, F. Desevedavy, L. Strizik, G. Gadret, P. Kalenda, B. Frumarova, L. Benes, S. Slang, M. Veis, T. Wagner, and F. Smektala, J. Non. Cryst. Solids 582 (2022) 121445
14. Q. Zhang, L. Han, W. Liu, W. You, A. Lu, and Z. Luo, J. Ceram. Process. Res. 22[1] (2021) 8-15.
15. R. Li, Q. Zhamg, X. Peng, and W. Liu, J. Ceram. Process. Res. 21[1] (2020) 86-91.
16. M. Takesue, H. Hayashi, and R.L. Smith Jr., Prog. Cryst. Growth Charact. Mater. 55[3-4] (2009) 98-124.
17. S.M. Abo-Naf and M.A. Marzouk, Nano-Structures & Nano-Objects 26 (2021) 100685.
18. S.A.M. Abdel-Hameed and F.H. Margha, Optik 206 (2020) 164374.
19. H.W. Leverenz, Science 109[2826] (1949) 183-195.
20. G.R. Fonda, J. Phys. Chem. 44[7] (1940) 851-861.
21. M.T. Tsai, Y.H. Lin, and J.R. Yang, Mater. Sci. Eng. 18 (2011) 032026.
22. A. Zatsepin, E. Buntov, N. Gavrilov, and H.J. Fitting, Phys. Status Solidi B 253[11] (2016) 2180-2184.
23. C.E. Rivera-Enríquez, A. Fernández-Osorio, and J. Chávez-Fernández, J. Alloys Compd. 688 (2016) 775-782.
24. M.H.M. Zaid, K.A. Matori, S.H.A. Aziz, H.M. Kamari, W.M.M. Yunus, Z.A. Wahab, and N.F. Samsudin, J. Spectrosc. 2016 (2016) 8084301.
25. A. Tarafder, A.R. Molla, S. Mukhopadhyay, and B. Karmakar, Opt. Mater. 36[9] (2014) 1463-1470.
26. N. Effendy, Z.A. Wahab, H.M. Kamari, K.A. Matori, S.H.A. Aziz, and M.H.M. Zaid, Optik 127[24] (2016) 11698-11705.
27. V. Lojpur, M.G. Nikolić, D. Jovanović, M. Medić, Ž. Antić, and M.D. Dramićanin, Appl. Phys. Lett. 103 (2013) 141912.
28. P. Yang, M.K. Lü, C.F. Song, S.W. Liu, F. Gu, and S.F. Wang, Inorg. Chem. Commun. 7[2] (2004) 268-270.
29. R. Ye, H. Ma, C. Zhang, Y. Gao, Y. Hua, D. Deng, P. Liu, and S. Xu, J. Alloys Compd. 566 (2013) 73-77.
30. T. Sakamoto, S. Kamei, K. Uematsu, T. Ishigaki, K. Toda, and M. Sato, J. Ceram. Process. Res. 14 (2013) s64-s66.
31. J.H. Zeng, H.L. Fu, T.J. Lou, Y. Yu, Y.H. Sun, and D.Y. Li, Mater. Res. Bull. 44[5] (2009) 1106-1110.
32. X. Ouyang, A.H. Kitai, and T. Xiao, J. Appl. Phys. 79 (1996) 3229-3234.
33. T.F. Veremeichik, E.V. Zharikov, and K.A. Subbotin, Crystallogr. Rep. 48[6] (2003) 974-988.
34. T.J. Lou, J.H. Zeng, X.D. Lou, H.L. Fu, Y.F. Wang, R.L. Ma, L.J. Tong, and Y.L. Chen, J. Colloid Interface Sci. 314[2] (2007) 510-513.
35. N.F. Samsudin, K.A. Matori, J.Y.C. Liew, Y.W. Fen, M.H.M. Zaid, and Z.N. Alassan, J. Spectrosc. (2015) 730753.
36. N.F. Samsudin, K.A. Matori, Z.A. Wahab, Y.W. Fen, J.Y.C. Liew, W.F. Lim, M.H.M. Zaid, and N.A.S. Omar, Appl. Opt. 55[9] (2016) 2182-2187.
37. B.C. Babu, B.V. Rao, M. Ravi, and S. Babu, J. Mol. Struct. 1127 (2017) 6-14.
38. K.M. Knowles and F.S.H.B. Freeman, J. Microsc. 215

(2004) 257-270.
39. J. Partyka and M. Leśniak, Ceram. Int. 42[7] (2016) 8513-8524.
40. S.K. Jung, C.H. Lee, C.H. Lee, and W.S. Cho, J. Ceram. Process. Res. 16[5] (2015) 525-530.
41. R. Casasola, J. M. Rincón, and M. Romero, J. Mater. Sci. 47 (2012) 553-582.
42. M. Li, J. Zou, G. Guo, J. Liu, and G. Wang, J. Ceram. Process. Res. 22[5] (2021) 504-509.
43. H.W. Choi, Y.H. Kim, Y.H. Rim, and Y.S. Yang, Phys. Chem. Chem. Phys. 15 (2013) 9940.
44. S. Saraswat, N. Mehta, and S.D. Sharma, J. Mater. Res. Technol. 5[2] (2016) 111-116.
45. S.M. Son and K.D. Kim, Ceram. Int. 49[9] (2023) 13677-13686.
46. J.A. Augis and J.E. Bennett, J. Therm. Anal. 13 (1978) 283-292.
47. Y.H. Na, Y.S. Kim, K.H. Lee, T.H. Kim, Y.J. Jung, N.J. Kim, S.H. Yim, and B.K. Ryu, J. Ceram. Process. Res. 10[2] (2009) 230-234.
48. Y.W. Lu, X.W. Du, J. Sun, X. Han, and S.A. Kulinich, J. Appl. Phys. 100 (2006) 063512.